



## Article

# Crack Propagation Behavior of Fused Silica during Cyclic Indentation under Incremental Loads

Koji Kosai <sup>1</sup>, Yugang Zhao <sup>2</sup> and Jiwang Yan <sup>1,\*</sup>

<sup>1</sup> Department of Mechanical Engineering, Faculty of Science and Technology, Keio University, Hiyoshi 3-14-1, Kohoku-ku, Yokohama 223-8522, Japan; koji.kosai@keio.jp

<sup>2</sup> School of Mechanical Engineering, Shandong University of Technology, Zibo 255000, China; zhaoyg9289@126.com

\* Correspondence: yan@mech.keio.ac.jp

**Abstract:** Fused silica is an important optical material with important applications, where the surface must be precisely machined without subsurface damage. In this study, multi-cyclic indentations under incremental loads were performed on fused silica using two kinds of indenters to clarify the mechanisms of crack generation and propagation induced by precision grinding. It was found that incremental loading cyclic nanoindentation induced various patterns of subsurface cracking and surface spalling. Four kinds of surface spalling were identified at different locations around an indent, the temporal formation mechanisms of which were clarified by microscopic observation and topographical measurement. Load–displacement curve analysis demonstrated that incremental propagation of lateral cracks during early indentation cycles caused large-scale brittle fractures during later cycles. Compared with a Berkovich indenter, a cube-corner indenter caused more significant brittle fractures and surface spalling. The findings in this study will deepen the understanding of subsurface damaging mechanism of fused silica and other brittle solids caused by cyclic tool-workpiece interactions in grinding and other mechanical machining processes.



**Citation:** Kosai, K.; Zhao, Y.; Yan, J. Crack Propagation Behavior of Fused Silica during Cyclic Indentation under Incremental Loads. *Appl. Sci.* **2022**, *12*, 6589. <https://doi.org/10.3390/app12136589>

Academic Editors: Xun Chen and James M. Griffin

Received: 19 May 2022

Accepted: 26 June 2022

Published: 29 June 2022

**Publisher's Note:** MDPI stays neutral with regard to jurisdictional claims in published maps and institutional affiliations.



**Copyright:** © 2022 by the authors. Licensee MDPI, Basel, Switzerland. This article is an open access article distributed under the terms and conditions of the Creative Commons Attribution (CC BY) license (<https://creativecommons.org/licenses/by/4.0/>).

**Keywords:** fused silica; micro/nano-indentation; cyclic load; hard brittle materials; subsurface damage; crack

## 1. Introduction

Fused silica possesses various excellent optical properties and is utilized for a wide range of applications including high-resolution imaging lenses for photolithography devices, laser communication, and space telescopes [1,2]. Fused silica optics are usually shaped by ultraprecision grinding and finished by polishing [3,4]. As fused silica is highly hard and brittle, cracks easily occur during grinding [5]. It takes a very long time to remove the grinding-induced cracks by subsequent polishing, and if the residual cracks cannot be completely removed, they will greatly affect the surface optical quality and the service life of the final products. Hence, clarification of the behavior and mechanism of crack initiation and propagation in fused silica is an extremely important step.

For investigating brittle fractures of materials in grinding processes, indentation experiments have been performed by various researchers attributed to the geometrical similarity between an indenter and an abrasive grain. It is well known that in indentation, brittle materials exhibit a characteristic crack system including median cracks, radial cracks, lateral cracks, and cone cracks [6,7]. The crack system in glass was confirmed by cross-sectional observation along the median/radial cracks [8–10]. Real-time observation of crack evolution during loading/unloading was also accomplished [6,11]. Furthermore, the indentation-induced crack generation mechanism has been used for understanding the subsurface damaging behaviors during abrasive machining processes [12–14].

The material removal model by grinding is schematically illustrated in Figure 1. Machining always starts from a subsurface damaged layer generated by the previous pass

of the abrasive grain, rather than from a fresh bulk region. As the depth of the preexisting cracks is usually deeper than the thickness of material removed by a single cut of an abrasive grain [15], the cracked layer is subjected to incrementally accumulated cyclic loads as the grinding wheel rotates. This situation causes a kind of accumulative historical effect in subsurface damage formation. However, most previous indentation studies focused on individual indentations, thus the effects of incremental-load cyclic loading/unloading still remains unknown. In recent years, cyclic indentation has been attempted on brittle single-crystalline materials such as silicon [16,17] and germanium [18,19], and it was demonstrated that multi-cyclic indentation induced completely different mechanical responses from that of individual indentations. For optical glasses, multi-cyclic indentation tests were performed by using Vickers indenters [20] and spherical indenters [21] to investigate fatigue properties, and the evolution of indentation-induced cracks during cyclic bending tests was also investigated [22]. However, all those experiments were performed under a constant maximum load; thus, the effect of incrementally increasing loads, which is closer to the actual grinding process, has not been clarified.

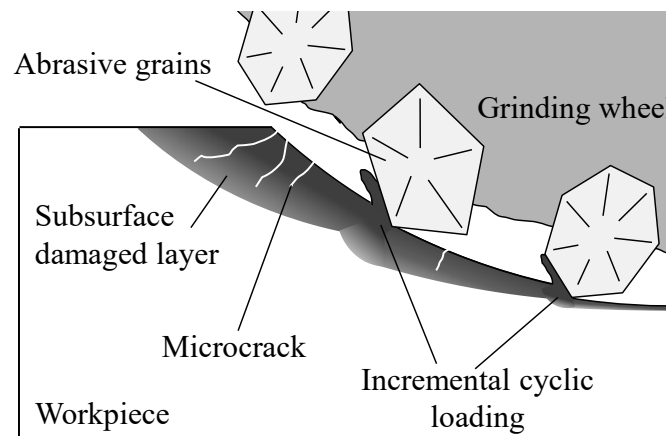


**Figure 1.** Schematic diagram of incremental cyclic loading in precision grinding of a hard brittle material.

In this study, multi-cyclic indentations with incrementally increasing maximum loads were performed on fused silica to investigate the material responses to cyclic loading/unloading, and the mechanisms of crack initiation and propagation were analyzed in detail. This study will deepen the understanding of cyclic load-induced subsurface damaging behaviors of high-hardness optical glass materials and other brittle solids in the micro/nanoscale, which is important for clarifying the ultraprecision grinding mechanisms and improving the machined surface quality.

## 2. Experimental Details

A fused silica plate was used as specimen, the major material properties of which (provided by the manufacturer) are listed in Table 1. As the indenter tip geometry affects the brittle fracture of glass materials [11,23–26], in this study, a Berkovich indenter and a cube-corner indenter made of single-crystal diamond were used for comparison. The geometries of the indenters are illustrated in Figure 2. The indentation tests were performed on a nanoindentation instrument ENT-1100a (Elionix Inc., Tokyo, Japan).

**Table 1.** Major material properties of the fused silica sample.

Material Properties	Values
Vickers hardness [GPa]	8.9
Young's modulus [GPa]	74
Poisson's ratio	0.17

**Table 1.** Cont.

Material Properties	Values
Bending strength [MPa]	94.3
Compressive strength [MPa]	1130
Size [mm]	$\Phi 10 \times 3$
OH content [ppm]	<200
Impurity	Ppb level

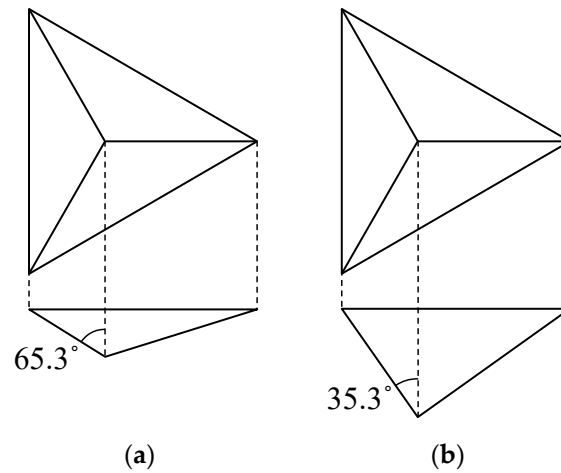


**Figure 2.** Indenter geometries used in this study: (a) Berkovich indenter; (b) cube-corner indenter.

Figure 3 illustrates the control graph of indentation load during incremental-load cyclic nanoindentation. At each indentation cycle, a constant loading/unloading rate was used, and the load was held for 1 s at the maximum load. The maximum load was increased by a constant step  $\Delta P$  between each indentation cycle and reached the final maximum load at the last cycle. After unloading of each cycle, the indenter tip was pulled up a few microns above the indented surface before the subsequent cycle started. To investigate the brittle fracture in micron and submicron-level, small maximum loads of 50 or 100 mN were applied. The number of indentation cycles were set to 2, 5, or 10 to comparatively examine the cyclic effects. For example, in incremental-load cyclic nanoindentation at a final maximum load of 100 mN with 10 cycles, the maximum load increased by  $\Delta P = 10$  mN between each cycle. For comparison, single nanoindentations were also carried out. To confirm reproductivity, the indentation tests were performed 10 times for each condition. Table 2 shows the indentation conditions.

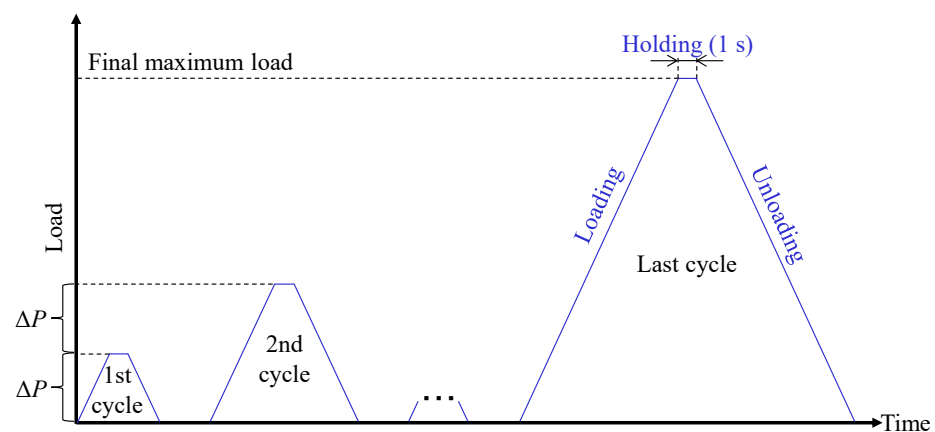


**Figure 3.** Control graph of indentation load for incremental cyclic nanoindentation.

**Table 2.** Incremental cyclic indentation conditions.

Indentation Parameters	Values
Final maximum load [mN]	50, 100
Loading/unloading rate [mN/s]	1
The number of indentation cycle	2, 5, 10
The number of tests at each condition	10
Indenter geometry	Berkovich, cube-corner
Indenter material	Single-crystal diamond

The indents were observed by using scanning electron microscopy (SEM), and the topography of the indent surface was examined by atomic force microscopy (AFM). Moreover, temporal analysis of deformation and brittle fracture during loading/unloading processes were performed based on the real-time recorded load–displacement curves.

### 3. Results and Discussion

#### 3.1. Observation of Indent Surface

Figures 4 and 5 show the SEM images of indents formed by the Berkovich indenter. Borderline cracks in curved shapes were observed around all the indents, as reported in previous studies [13,25]. Borderline crack traces were also observed inside the indents, which had been formed during the early cycles. However, there was no surface spalling due to crack propagation. This fact implies that incremental-load cyclic indentation by a Berkovich indenter induces multiple borderline cracks but does not propagate the cracks formed during the early cycles.

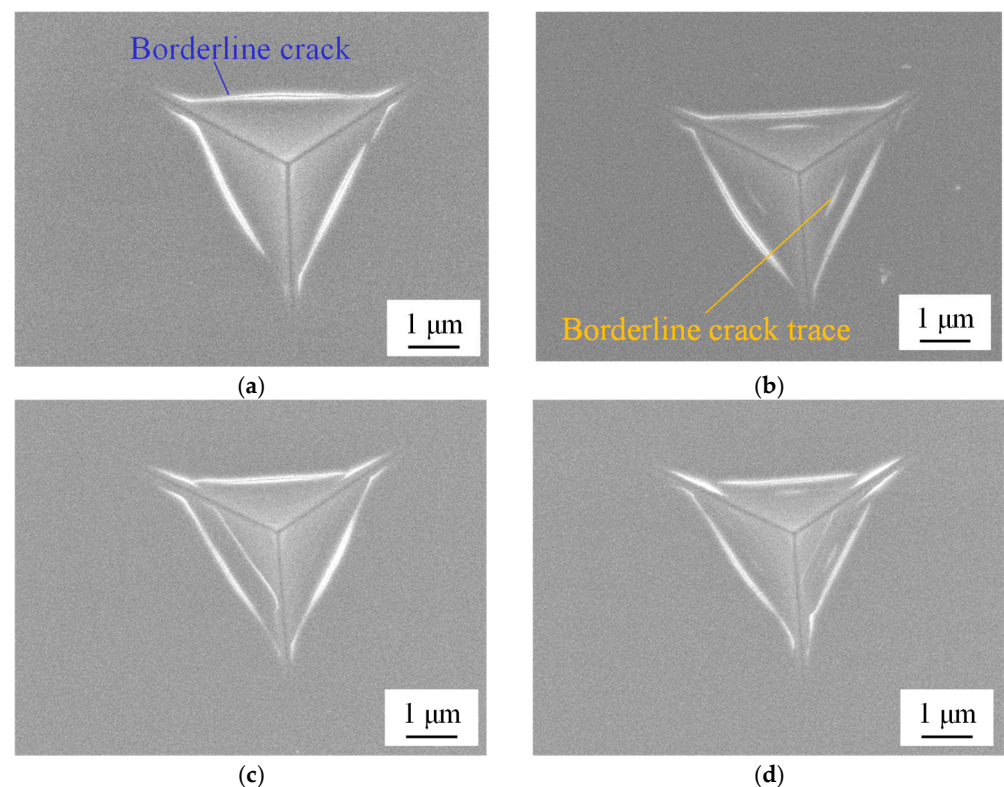


**Figure 4.** SEM images of indents generated by a Berkovich indenter at 100 mN: (a) single; (b) 2 cycles; (c) 5 cycles; (d) 10 cycles.

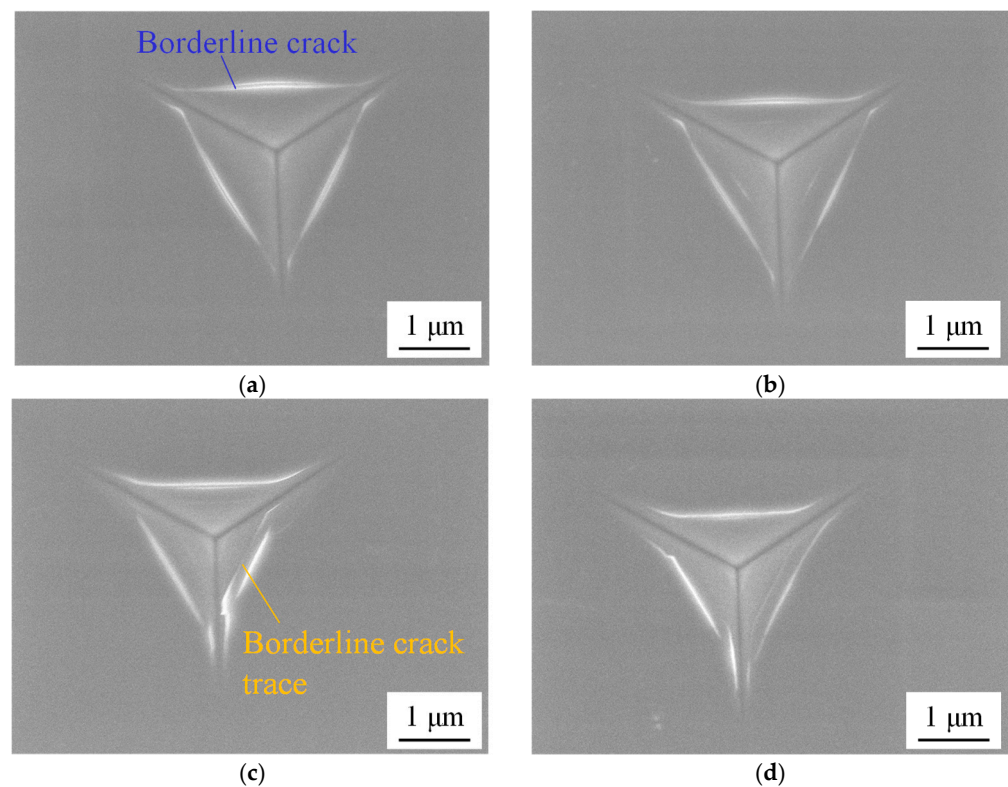


**Figure 5.** SEM images of indents generated by a Berkovich indenter at 50 mN: (a) single; (b) 2 cycles; (c) 5 cycles; (d) 10 cycles.

Incremental-load cyclic indentation by the cube-corner indenter caused various types of brittle fractures, as shown in Figures 6 and 7. For all indents, long radial cracks were observed around the indent edges. For multi-cyclic indentations (Figures 6b–d and 7c–e), surface spalling was confirmed around the indents, which was not observed for single indentation (Figures 6a and 7a) and two-cycle indentation (Figure 7b). This aspect is distinctly different from that of the indents made by the Berkovich indenter. As the maximum load increases, four different kinds of surface spalling were identified. The most popular surface spalling is fan-shaped, the profile of which is composed of a large arc, two radial cracks and an indent edge (for example see Figure 6b). This type of spalling is termed deep spalling, as the large arc indicates that it is caused by deep lateral crack propagation. The second type is small internal spalling which occurs inside the indent (for example, see Figure 6c). This type of surface spalling has an irregular shape and might be a result of the detachment of a plastically deformed layer near the indent surface. The third type, termed secondary spalling, has an elliptical shape which is closely connected to first type (for example, see Figure 6d). It is presumable that the secondary spalling is caused by the propagation of the first type. In addition, the fourth type of surface spalling was confirmed for some indents such as the one in Figure 7e. This type of spalling takes place inside the first type, near the edge of indenter. The size of spalling is small, indicating that it is caused by shallow lateral cracks, and thus, it is named shallow spalling.

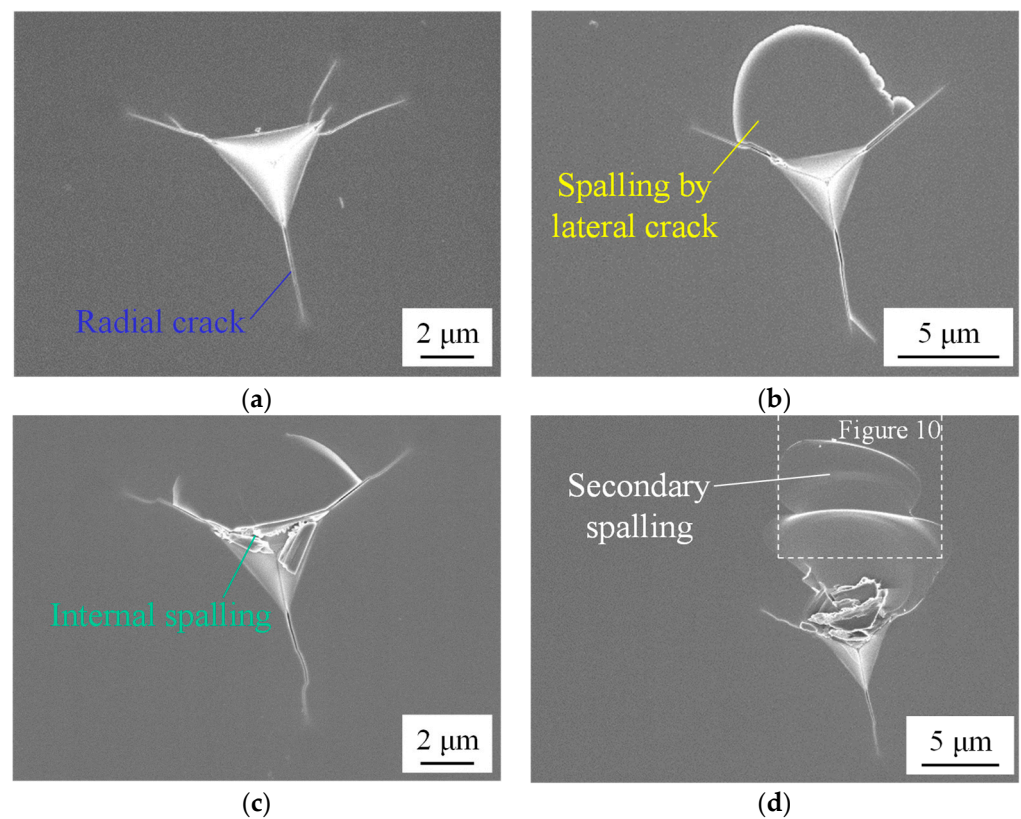


**Figure 6.** SEM images of indents generated by a cube-corner indenter at 100 mN: (a) single; (b) 2 cycles; (c) 5 cycles; (d) 10 cycles.

Surface spalling is a result of lateral crack propagation during unloading [11]. The process of crack initiation, propagation and spalling was observed by using a CCD camera. Figure 8 shows CCD images of the same indents as those shown in Figure 6. For a single indentation (Figure 8a), although lateral cracks were initiated beneath the surface, the cracks did not propagate further. As the indentation cycle increases, the lateral cracks propagate in the subsurface region, causing the size and brightness of the shining areas to increase. Interference fringes are observed (Figure 8b), indicating the formation of big gaps beneath the surface. As indentation cycle further increases, complete spalling occurs, and the material pieces are removed from the surface, leaving dark craters (Figure 8d). From these results, it is concluded that incremental cyclic indentation causes significant lateral crack propagation, which in turn leads to surface spalling.

For quantitative evaluation of the effect of loading methods, the incidence of complete spalling at each indentation condition was calculated as shown in Figure 9. In the calculation, spalling with partial connection to the bulk, like that shown in Figure 6c, was not regarded as a complete spalling. The single indentation was not listed in Figure 9 due to there being no occurrence of complete spalling. Figure 9 demonstrates that incremental-load cyclic indentation with more cycles promoted spalling regardless of the maximum load. After 10 cycles, there was no difference between maximum loads of 100 and 50 mN. This result indicates again that in incremental-load cyclic indentation by a cube-corner indenter, lateral crack propagation was promoted to cause spalling. It should be mentioned that in the cases of the Berkovich indenter, no spalling was observed even at incremental-load cyclic indentation after 10 cycles.

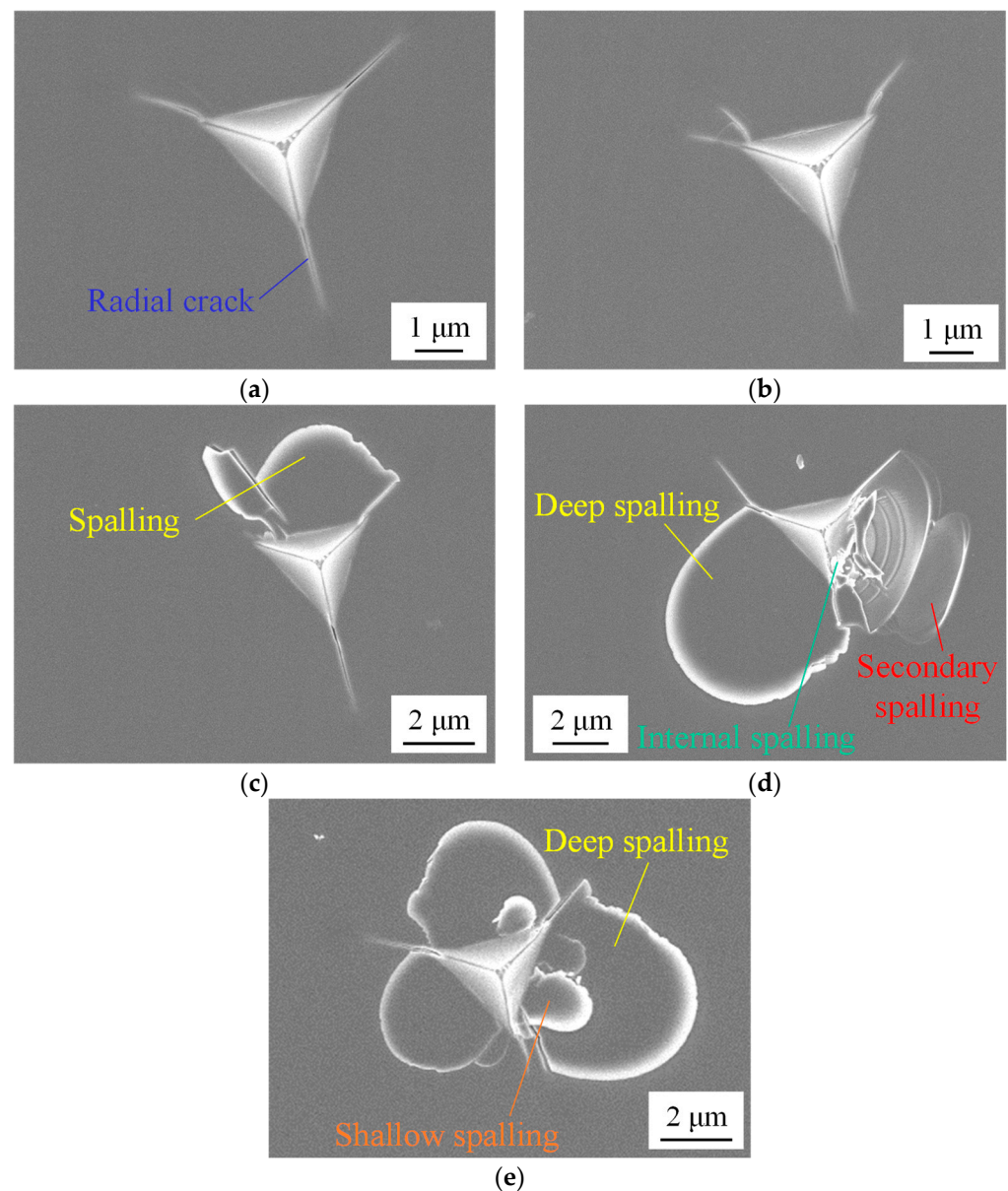


**Figure 7.** SEM images of indents generated by a cube-corner indenter at 50 mN: (a) single; (b) 2 cycles; (c) 5 cycles; (d) 10 cycles; (e) 10 cycles.

Figure 10 shows a detailed surface topography of the secondary spalling in Figure 6d, measured by AFM. As can be seen in the 3D image in Figure 10b and the cross-sectional profile in Figure 10c, there is a steep step at the crater edge between the deep spalling and the secondary spalling. This fact indicates that discontinuous crack propagation has occurred with the initiation of the secondary spalling.

### 3.2. Load–Displacement Curve Analysis

To investigate temporal deformation/fracture behaviors of material during incremental cyclic indentation, load–displacement curve analysis was performed. Figures 11 and 12 are load–displacement curves of indentations made by the Berkovich indenter at maximum loads of 100 mN and 50 mN, respectively. For both figures, the loading curves of multiple cycles overlapped partially, and the slopes of the unloading curves were very similar. No features such as pop-in and pop-out on the curves were observed, indicating that indentation by the Berkovich indenter did not induce significant detachment of a surface layer due to cracks.

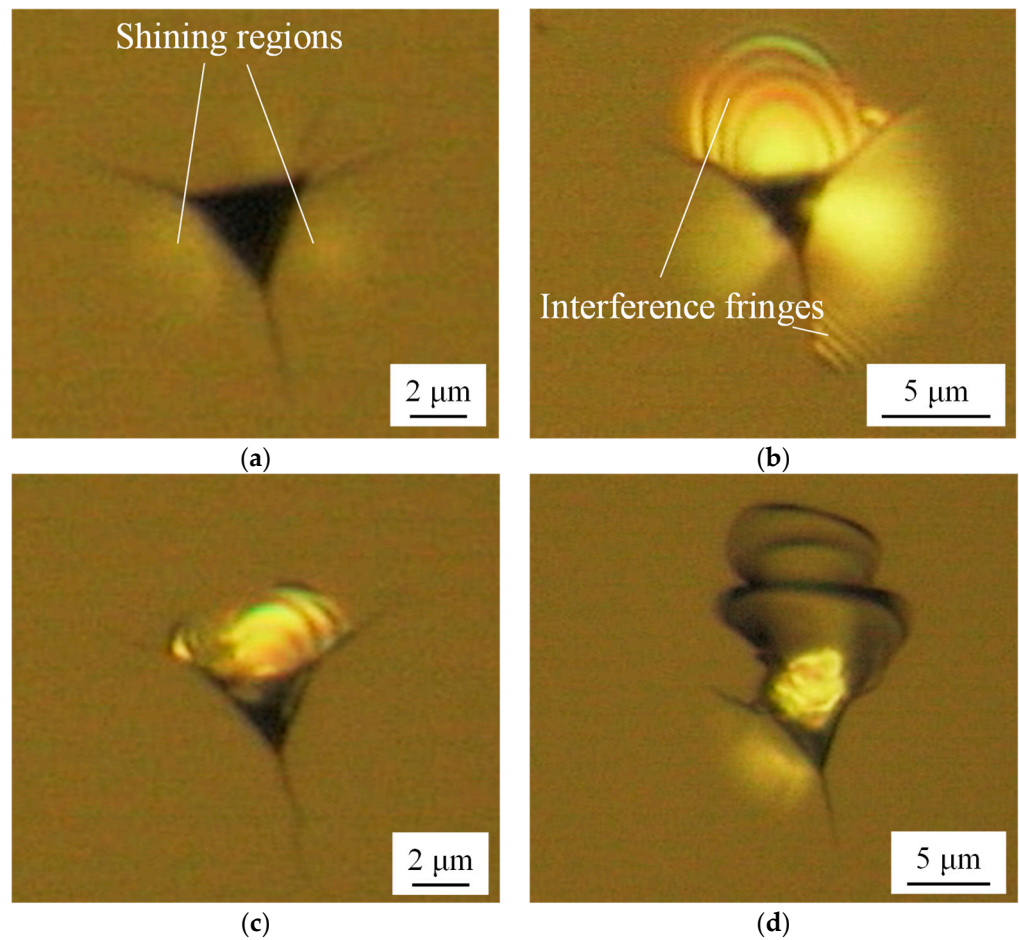


**Figure 8.** CCD camera images of indents shown in Figure 6 which were generated by a cube-corner indenter at 100 mN: (a) single; (b) 2 cycles; (c) 5 cycles; (d) 10 cycles. The shining areas and interference fringes indicate lateral crack propagation in the subsurface regions.

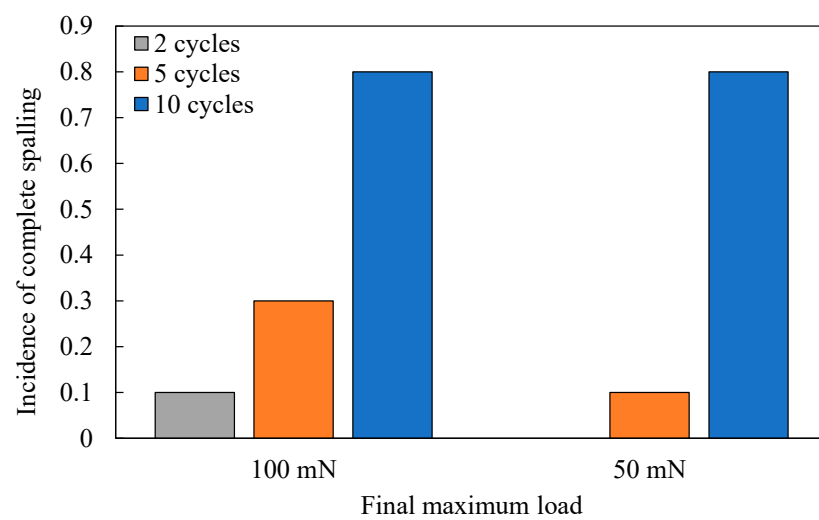


**Figure 9.** Incidence of complete spalling for each incremental cyclic indentation condition.



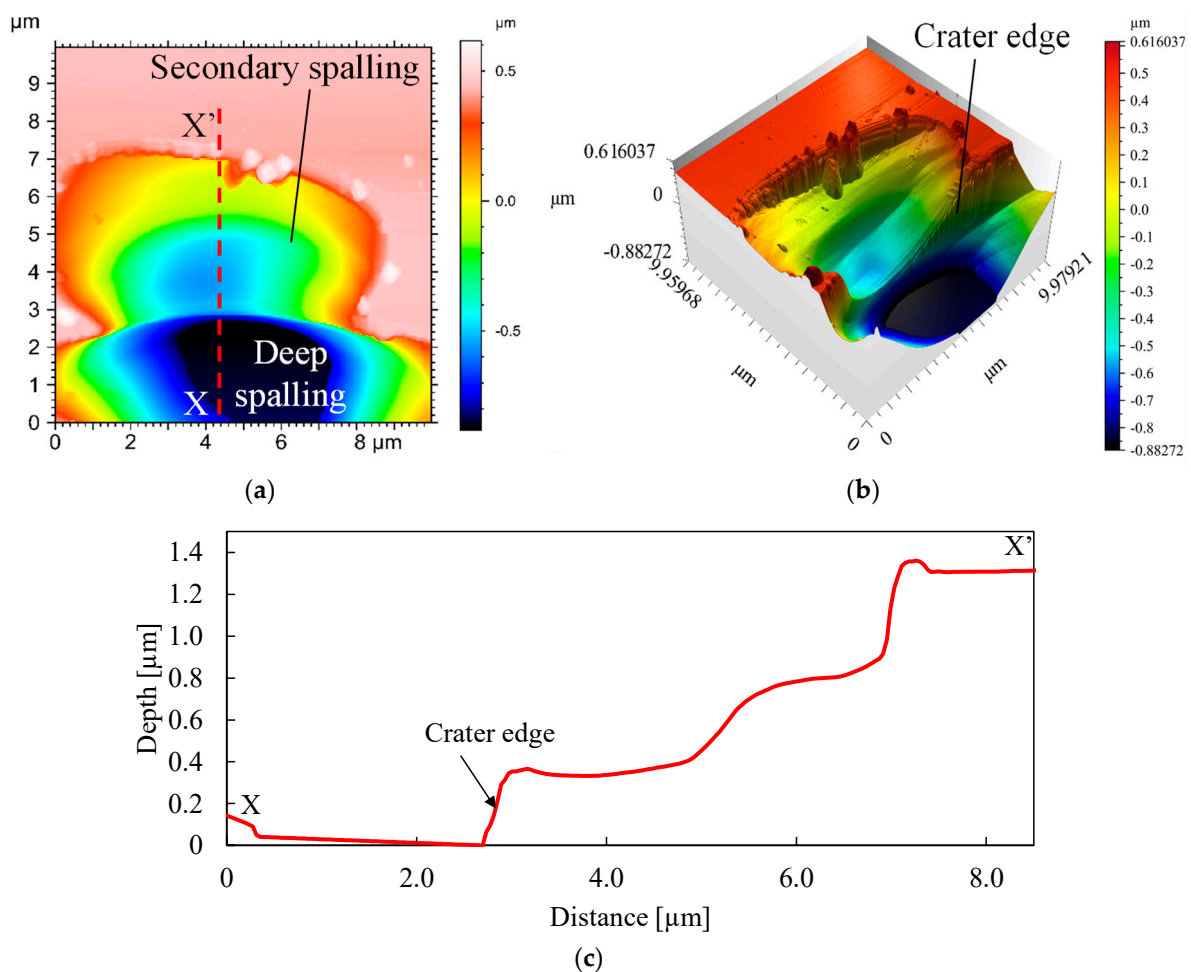


**Figure 10.** Surface topography around the secondary spalling in Figure 6d: (a) 2D and (b) 3D images; (c) cross-sectional profile of the spalling along the dotted line in (a).

Figures 13 and 14 illustrate load displacement curves of incremental cyclic indentations by the cube-corner indenter at maximum loads of 100 mN and 50 mN, respectively. As compared to the curves of the Berkovich indenter in Figures 11 and 12, there are some characteristic features. First, all the unloading curves exhibit elbows, namely, discrete changes in slope, at the last parts of unloading curves. An elbow means promoted displacement decrease by some factors such as phase transformation with volume expansion [26,27] and detachment of a surface layer like a coating beneath the indenter [28,29].

The elbows were more clearly observed via the slope changes of the tangential lines on the unloading curves as shown in Figure 15. For the Berkovich indenter, the slope decreases and the decreasing speed becomes faster as unloading progresses ((a) (b)). On the other hand, for the cube-corner indenter, the slope decrease becomes discrete and slower at the end parts ( $\sim 20$  mN for (c) and  $\sim 6$  mN for (d)), which is the evidence of elbows. In this study, the elbow would be caused by surface spalling, i.e., detachment of a surface layer due to lateral crack propagation. This agrees with the result that the incremental-load cyclic indentation significantly promoted lateral crack propagation, as shown by the SEM observations. Due to the occurrence of elbow, the overlapping phenomenon of loading/unloading curves in Figures 11 and 12 was not observed in Figures 13 and 14. The repetitive occurrence of elbow indicates incremental propagation of lateral cracks and surface spalling, as shown in Figure 9.

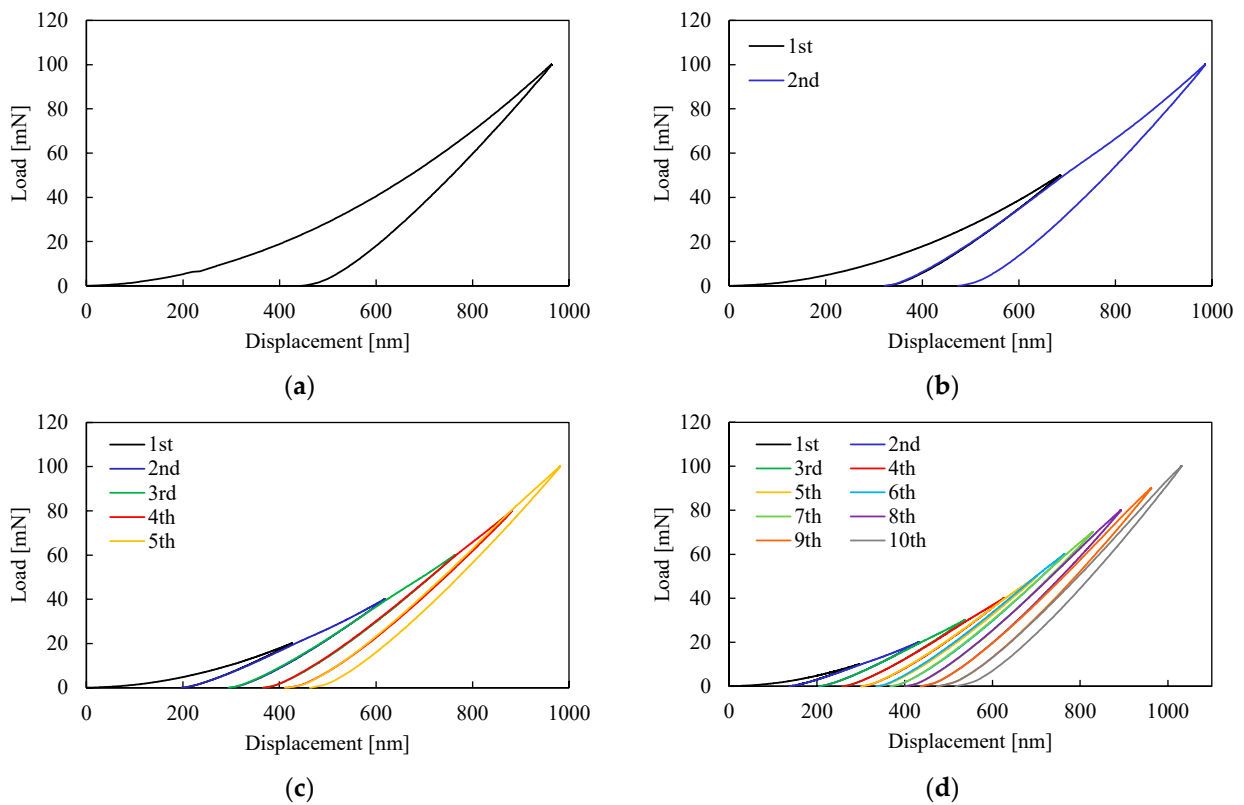


**Figure 11.** Load–displacement curves recorded during indentations using a Berkovich indenter at 100 mN: (a) single; (b) 2 cycles; (c) 5 cycles; (d) 10 cycles, corresponding to the SEM images in Figure 4.

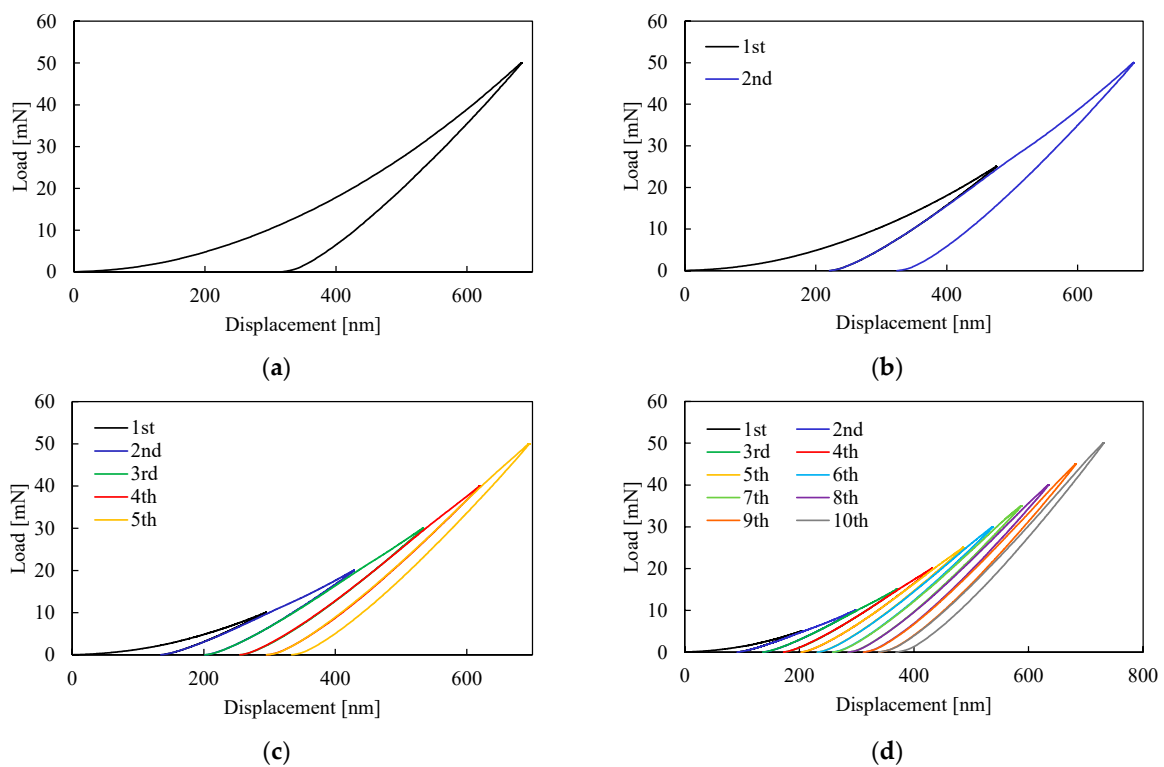


**Figure 12.** Load–displacement curves recorded during indentations by a Berkovich indenter at 50 mN: (a) single; (b) 2 cycles; (c) 5 cycles; (d) 10 cycles, corresponding to the SEM images in Figure 5.

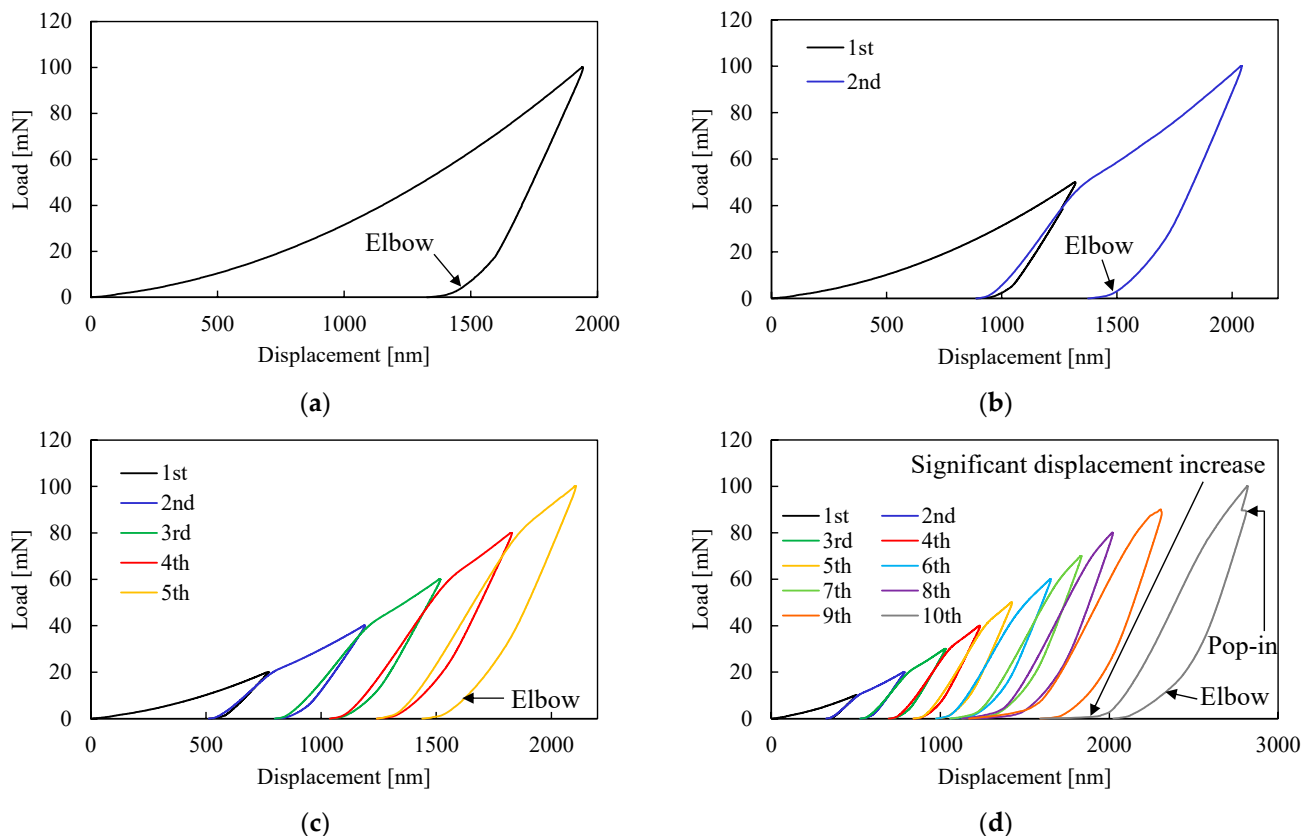


**Figure 13.** Load–displacement curves recorded during indentations by a cube-corner indenter at 100 mN: (a) single; (b) 2 cycles; (c) 5 cycles; (d) 10 cycles, corresponding to the SEM images in Figure 6.

Another feature of the load–displacement curve is the occurrence of pop-ins. In Figures 13d and 14d, pop-ins were observed. A pop-in is known as a result of radial crack formation, although radial crack formation does not always result in a pop-in [23]. Pop-ins usually occur during loading. It has been also reported that a cube-corner indenter induces pop-ins during unloading due to the wedging [23,24]. The big pop-in observed during unloading in Figure 13d might be based on the wedging. The spalling around the indents causes material removal from the surface, which decreases the resistance against the wedging, and in turn, increases the size of a pop-in.

Moreover, there was a discrete displacement increase at the initial part of loading on later cycles of some incremental-load cyclic indentations, as shown in Figures 13d and 14d. Such displacement increase was not observed during the early cycles. For quantitatively evaluating the occurrence of the initial displacement increase, the ratio of  $P'$  and  $P$  ( $P'$ : the load at the intersection point between two cycles;  $P$ : the previous maximum load) was calculated as Figure 16, where the definition of the ratio is given in the subfigure. If the initial displacement increase is significant,  $P'$  becomes lower since the loading curves are shifted to the right side. In Figure 16, the ratio increases and then decreases as the indentation cycle increases, indicating that the initial displacement increase occurs during the later cycles.

It is noted that the standard distribution during later cycles in Figure 16 is bigger than that of early cycles. This is because as the indentation cycle increases, the divergence of crack generation pattern increases too. As confirmed in Figure 7d,e, even under the same conditions, different fracture patterns lead to significantly different shapes of load–displacement curves, as shown in Figure 14d,e. The big initial displacement increase in Figure 14d might be caused by the crush of the internal spalling fragments sandwiched by the indenter and sample.

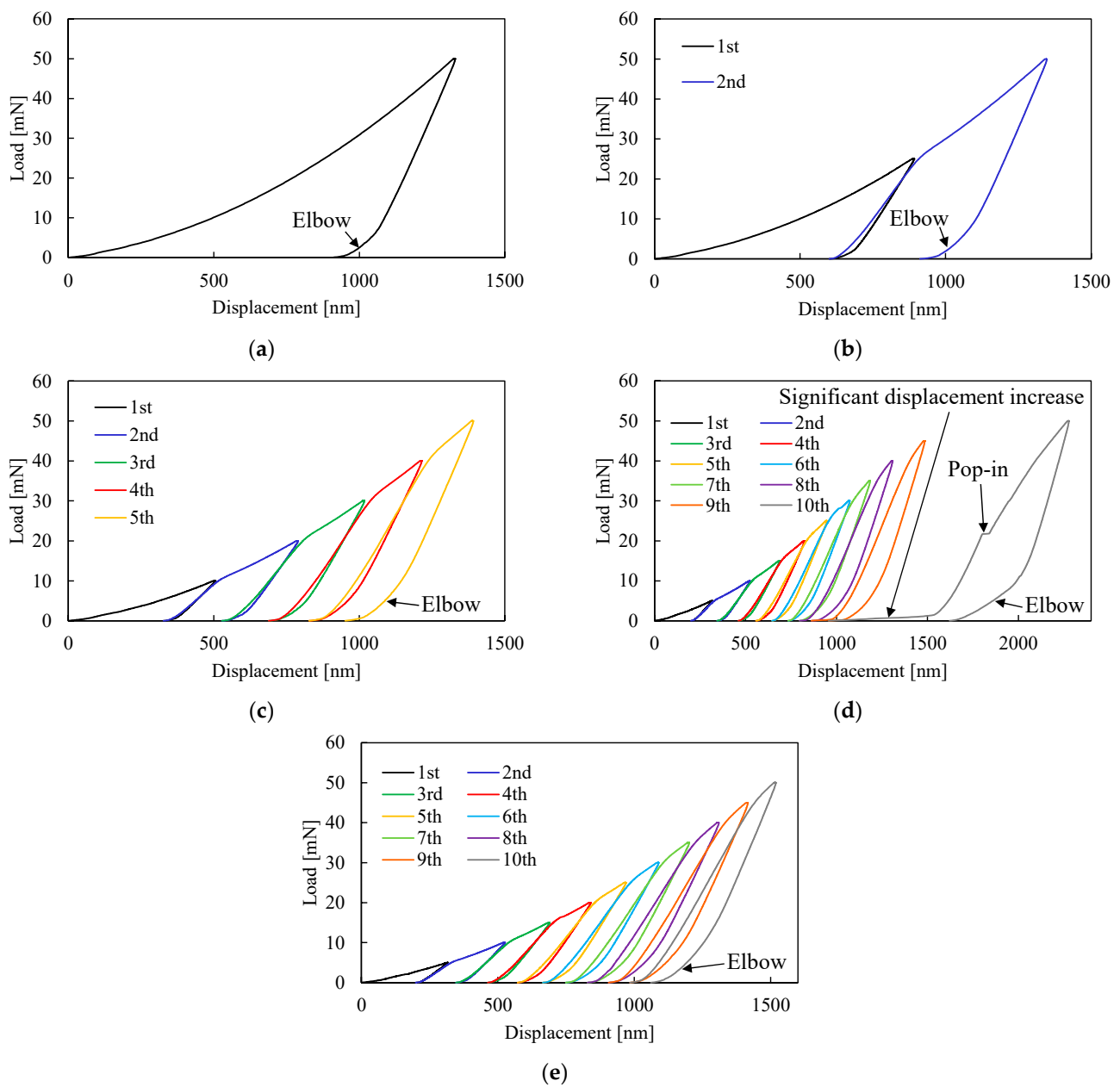


**Figure 14.** Load–displacement curves recorded during indentations by a cube-corner indenter at 50 mN: (a) single; (b) 2 cycles; (c) 5 cycles; (d) 10 cycles; (e) 10 cycles, corresponding to the SEM images in Figure 7.

### 3.3. Crack Generation/Propagation Mechanisms

Based on the above-mentioned results and analysis, the mechanisms of cracking behaviors in incremental-load cyclic indentation are discussed as follows. First, the load–displacement curves showed repetitive elbows during unloading, which indicates occurrence of multiple lateral cracks. A lateral crack initiates beneath the plastic region beneath an indenter [11,30,31]. During incremental-load cyclic indentation, the plastic region expands with increasing maximum load and indentation depth. Therefore, new lateral cracks may initiate and propagate beneath the expanded plastic region during later cycles. As schematically illustrated in Figure 17, the newly formed lateral crack in the  $n_2$ th cycle will be deeper than the that formed in an early  $n_1$ th cycle. An early lateral crack causes shallow spalling while a crack occurring in the later stage leads to deep spalling. In addition, the generation of multiple lateral cracks may result in spalling inside the indents. As the inden-

tation depth increases, the shallow lateral cracks are affected by the plastic deformation caused by the later indentation cycles. The loading-induced densification and unloading-induced elastic spring-back become significant in the indentation of silica glass [32]. Due to these cyclic deformations, internal spalling occurs, as observed in Figures 6c,d and 7d.

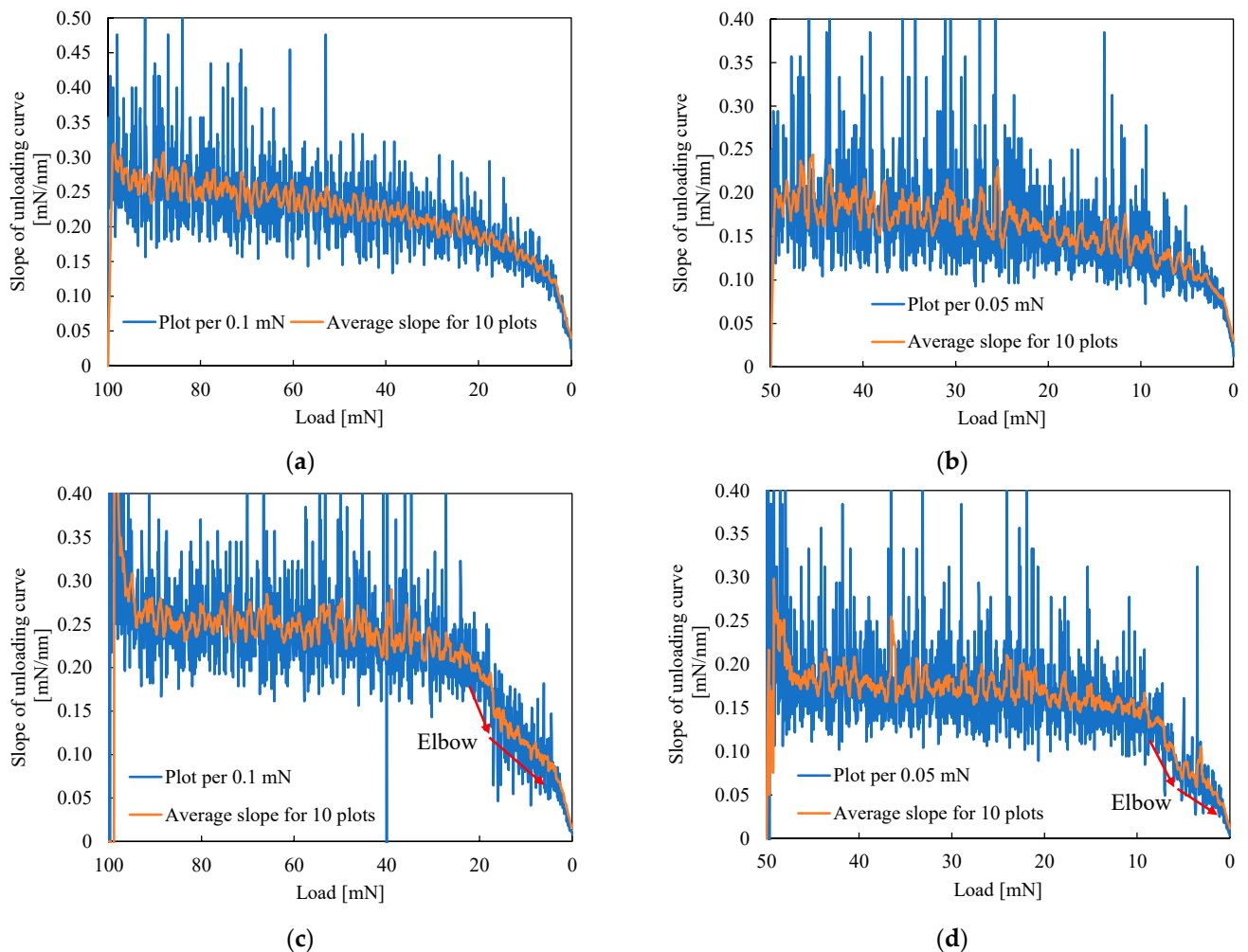


**Figure 15.** Change in slope of unloading curve during single indentations: (a) 100 mN, Berkovich (Figure 11a); (b) 50 mN, Berkovich (Figure 12a); (c) 100 mN, cube-corner (Figure 13a); (d) 50 mN, cube-corner (Figure 14a).

Another characteristic brittle fracture induced by incremental-load cyclic indentation is secondary spalling as shown in Figures 6d and 7d. As the secondary spalling occurs at a distant region from the indent, the direct cause of it may not be the indenter itself. Instead, it might be caused by the fragment of deep spalling which behaves as an expanding core under compression from the indenter. As illustrated in Figure 18, in later cycles, the fragment piece generated by a deep spalling is compressed by the indenter and pushed toward the outer area. The lateral compression force from the indenter is transferred by the fragment to the crater edge step of the deep spalling, causing the occurrence of secondary spalling. Such a situation is similar to loading a blunt indenter to the outer material, which induces new lateral crack initiation along spreading direction, and in turn, a secondary spalling.

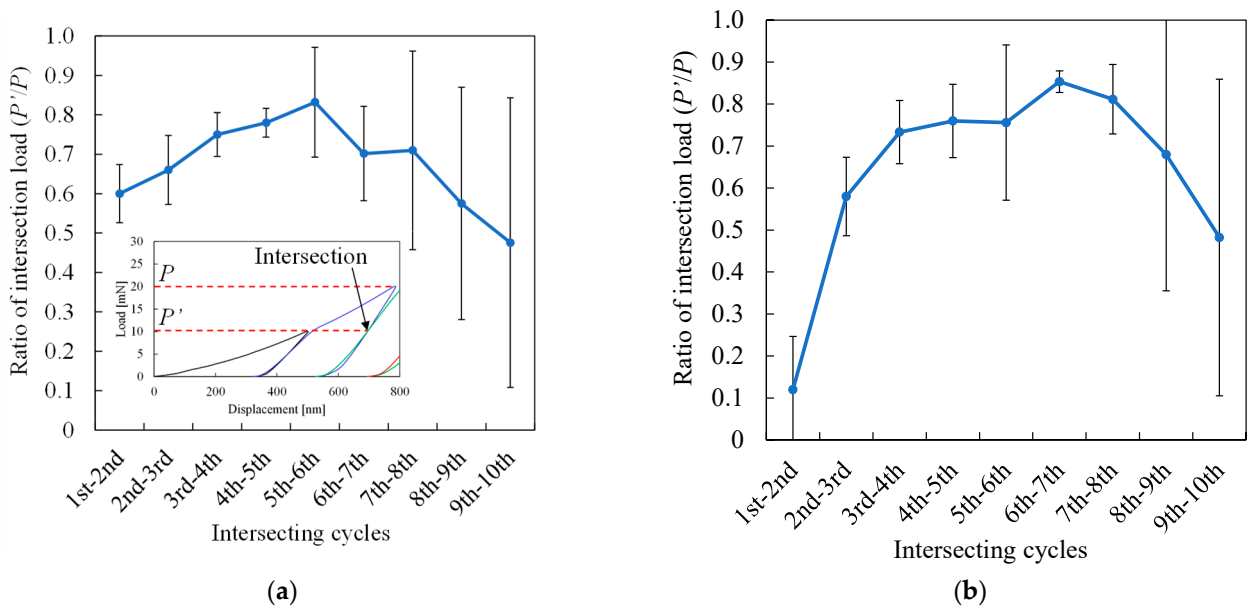


**Figure 16.** Ratio of  $P'$  and  $P$  ( $P'$ : load at the intersection between two cycles;  $P$ : the maximum load of the previous cycle) in incremental cyclic indentation by a cube-corner indenter at maximum loads of (a) 100 mN and (b) 50 mN. The subfigure in (a) explains the definition of  $P'$  and  $P$ .

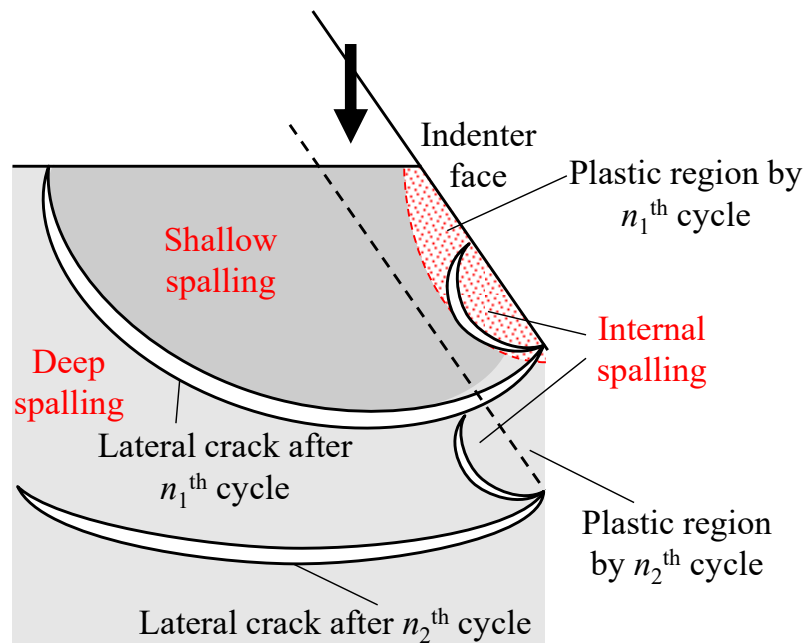


**Figure 17.** Schematic cross-sectional view of various spalling patterns in early stage of incremental cyclic indentation.

Based on the aforementioned analysis, a schematic diagram of temporal cracking/spalling behavior during incremental-load cyclic indentation using a cube-corner indenter is illustrated in Figure 19. On loading of early cycles, median/radial cracks initiate and propagate, and a plastic region is also formed beneath the indenter (Figure 19a). On unloading, lateral cracks initiate and propagate beneath the plastic region (Figure 19b). In a single Vickers indentation, lateral cracks propagate in semicircular median/radial cracks [10] or along the bottom of semielliptical medial/radial cracks with interrupting further median/radial crack propagation to the depth direction [8]. The lateral crack propagates on unloading, but enough large load can induce lateral cracking even on loading [11]. In such a case, the lateral crack can interrupt further propagation of radial/median cracks

in the depth direction, resulting in semielliptical medial/radial cracks. In the early cycles of incremental-load cyclic indentation, the indentation load was very small, so the lateral cracks would form during only unloading. Hence, the shape of median/radial cracks around the indent edges should be quarter circular containing lateral cracks. As the indentation cycle increases, expansion of the plastic region and propagation of median/radial cracks progress during loading (Figure 19c). During unloading, in addition to the propagation of lateral cracks formed on earlier cycles, new lateral cracks initiate beneath the expanded plastic region (Figure 19d). The lateral cracks propagate, resulting spalling fractures. If the fragment of spalling is not removed, the subsequent loading will cause the lateral cracks to close, and thus the lateral compression from the indenter is transferred to the outer region via the fragment, forming an expanding core. A new lateral crack is then initiated and propagates in the outer region, forming the secondary spreading (Figure 19e).

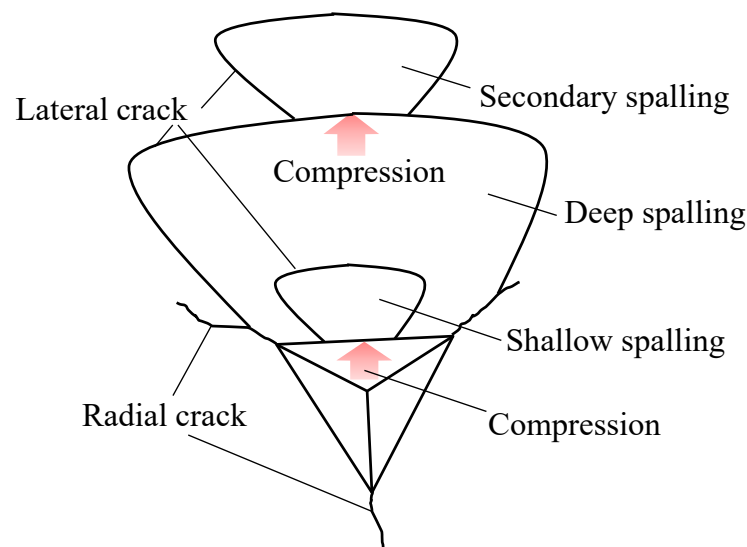


**Figure 18.** Schematic top view of secondary spalling formation in later stage of incremental cyclic indentation.

The clarification of cracking/spalling behavior during incremental-load cyclic indentation is very useful for understanding the mechanisms of abrasive machining, especially the grinding of hard brittle materials for high-precision optics fabrication [33–35]. The characteristic crack propagation and spalling fractures observed in this study provide direct reference for understanding the subsurface damage formation and material removal mechanism under incremental cyclic loads, as shown in Figure 1. The findings will close the gap in the understanding of microscopic fracture phenomena during real micro/nanoscale processing of optical glass and other brittle materials, as it is extremely difficult for in situ observation of these high-speed processes. If the correlation between cyclic nanoindentation and grinding is clearly established, it will greatly contribute to the process optimization of grinding technology for advanced optical components.

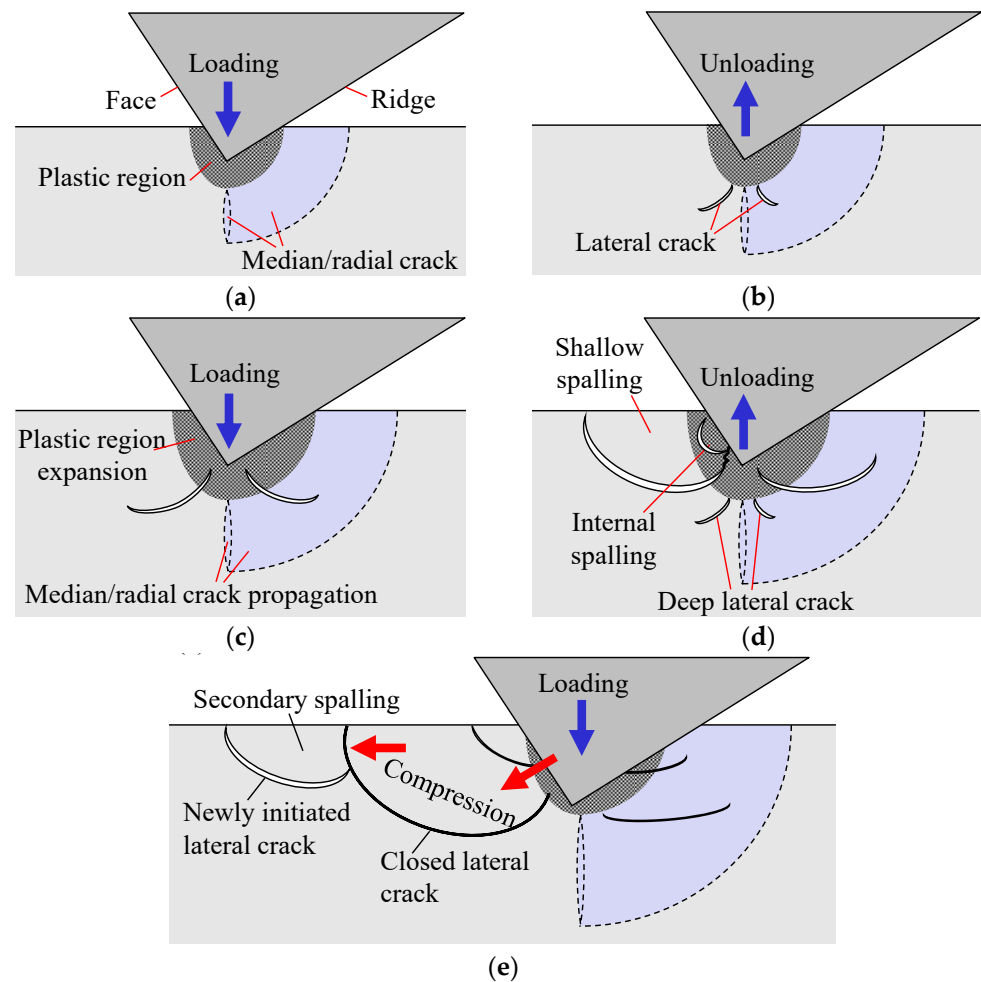


**Figure 19.** Schematic diagram of cracking/spalling behavior during incremental cyclic indentation using a cube-corner indenter: (a) loading and (b) unloading in early cycles; (c) loading and (d) unloading in later cycles; (e) loading in final stage.

#### 4. Conclusions

Incremental-load cyclic nanoindentation tests were carried out on fused silica, and brittle microfracture phenomena were examined by SEM observation, AFM measurement as well as load–displacement curve analysis. The following conclusions were obtained:

- (1) Surface spalling becomes significant as indentation cycle increases when a cube-corner indenter is used, while a Berkovich indenter induces no surface spalling under the present experimental conditions.
- (2) Four types of characteristic patterns of surface spalling were identified: shallow spalling, deep spalling, internal spalling, and secondary spalling. The latter three kinds of spalling patterns only occur in incremental-load cyclic indentations.
- (3) The load–displacement curves exhibit unique features such as repetitive elbows, large pop-ins and significant displacement increase at the initial part of loading, which correspond to the incremental propagation of lateral cracks and surface spalling.
- (4) Multi-cyclic indentation using a cube-corner indenter promotes subsurface crack propagation and surface spalling (material removal) both in depth direction and in lateral direction compared to single-cycle indentation.

This study reveals the mechanism of microscopic brittle fractures in optical glass induced by cyclic loading/unloading, which is distinctly different from that reported by previous studies in single indentation tests. The findings provide new insights in subsurface damaging and material removal behaviors under cyclic loads, which will help clarify the



mechanism of micro/nanoscale machining processes such as grinding. One of the future directions is to establish the correlations between cyclic indentation and precision grinding, based on which, the optimization of the grinding parameters may be possible to suppress subsurface damage formation and achieve high-quality optical surfaces.

**Author Contributions:** Conceptualization, K.K. and J.Y.; methodology, K.K.; investigation, K.K.; writing—original draft preparation, K.K.; writing—review and editing, Y.Z. and J.Y.; visualization, K.K., Y.Z. and J.Y.; supervision, J.Y. All authors have read and agreed to the published version of the manuscript.

**Funding:** This research received no external funding.

**Institutional Review Board Statement:** Not applicable.

**Informed Consent Statement:** Not applicable.

**Data Availability Statement:** Not applicable.

**Conflicts of Interest:** The authors declare no conflict of interest.

## References

1. Fang, F.Z.; Zhang, X.D.; Weckenmann, A.; Zhang, G.X.; Evans, C. Manufacturing and measurement of freeform optics. *CIRP Ann. Manuf. Technol.* **2013**, *62*, 823–846. [[CrossRef](#)]
2. Kakinuma, Y.; Konuma, Y.; Fukuta, M.; Tanaka, K. Ultra-precision grinding of optical glass lenses with La-doped CeO<sub>2</sub> slurry. *CIRP Ann.* **2019**, *68*, 345–348. [[CrossRef](#)]
3. Li, S.; Wang, Z.; Wu, Y. Relationship between subsurface damage and surface roughness of optical materials in grinding and lapping processes. *J. Mater. Process. Technol.* **2008**, *205*, 34–41. [[CrossRef](#)]
4. Suratwala, T.; Steele, R.; Feit, M.D.; Wong, L.; Miller, P.; Menapace, J.; Davis, P. Effect of rogue particles on the sub-surface damage of fused silica during grinding/polishing. *J. Non-Cryst. Solids* **2008**, *354*, 2023–2037. [[CrossRef](#)]
5. Wang, J.; Li, Y.; Han, J.; Xu, Q.; Guo, Y. Evaluating subsurface damage in optical glasses. *J. Eur. Opt. Soc.* **2011**, *6*, 11011. [[CrossRef](#)]
6. Cook, R.F.; Pharr, G.M. Direct Observation and Analysis of Indentation Cracking in Glasses and Ceramics. *J. Am. Ceram. Soc.* **1990**, *73*, 787–817. [[CrossRef](#)]
7. Elfallagh, F.; Inkson, B.J. 3D analysis of crack morphologies in silicate glass using FIB tomography. *J. Eur. Ceram. Soc.* **2009**, *29*, 47–52. [[CrossRef](#)]
8. Whittle, B.R.; Hand, R.J. Morphology of Vickers Indent Flaws in Soda-Lime-Silica Glass. *J. Am. Ceram. Soc.* **2001**, *84*, 2361–2365. [[CrossRef](#)]
9. Li, C.; Zhang, L.; Sun, L.; Yang, S.; Wu, C.; Long, X.; Ding, J.; Jiang, Z. A quantitative analysis of the indentation fracture of fused silica. *J. Am. Ceram. Soc.* **2019**, *102*, 7264–7277. [[CrossRef](#)]
10. Januchta, K.; Liu, P.; Hansen, S.R.; To, T.; Smedskjaer, M.M. Indentation cracking and deformation mechanism of sodium aluminoborosilicate glasses. *J. Am. Ceram. Soc.* **2020**, *103*, 1656–1665. [[CrossRef](#)]
11. Morris, D.J.; Cook, R.F. In situ cube-corner indentation of soda-lime glass and fused silica. *J. Am. Ceram. Soc.* **2004**, *87*, 1494–1501. [[CrossRef](#)]
12. Suratwala, T.; Wong, L.; Miller, P.; Feit, M.D.; Menapace, J.; Steele, R.; Davis, P.; Walmer, D. Sub-surface mechanical damage distributions during grinding of fused silica. *J. Non-Cryst. Solids* **2006**, *352*, 5601–5617. [[CrossRef](#)]
13. Wang, W.; Yao, P.; Wang, J.; Huang, C.; Zhu, H.; Zou, B.; Liu, H.; Yan, J. Crack-free ductile mode grinding of fused silica under controllable dry grinding conditions. *Int. J. Mach. Tools Manuf.* **2016**, *109*, 126–136. [[CrossRef](#)]
14. Li, P.; Chen, S.; Xiao, H.; Chen, Z.; Qu, M.; Dai, H.; Jin, T. Effects of local strain rate and temperature on the workpiece subsurface damage in grinding of optical glass. *Int. J. Mech. Sci.* **2020**, *182*, 105737. [[CrossRef](#)]
15. Chen, J.; Fang, Q.; Li, P. Effect of grinding wheel spindle vibration on surface roughness and subsurface damage in brittle material grinding. *Int. J. Mach. Tools Manuf.* **2015**, *91*, 12–23. [[CrossRef](#)]
16. Huang, H.; Yan, J. On the mechanism of secondary pop-out in cyclic nanoindentation of single-crystal silicon. *J. Mater. Res.* **2015**, *30*, 1861–1868. [[CrossRef](#)]
17. Huang, H.; Yan, J. New insights into phase transformations in single crystal silicon by controlled cyclic nanoindentation. *Scr. Mater.* **2015**, *102*, 35–38. [[CrossRef](#)]
18. Kosai, K.; Huang, H.; Yan, J. Comparative Study of Phase Transformation in Single-Crystal Germanium during Single and Cyclic Nanoindentation. *Crystals* **2017**, *7*, 333. [[CrossRef](#)]
19. Kosai, K.; Yan, J. Direct observations of multi-cyclic nanoindentation-induced phase transformations in single-crystal Ge. *Mater. Res. Express* **2019**, *6*, 75065. [[CrossRef](#)]
20. Banerjee, R.; Sarkar, B.K. Crack initiation by indentation fatigue in lead alkali and soda-lime glass. *J. Am. Ceram. Soc.* **1997**, *80*, 2722–2724. [[CrossRef](#)]

21. Kim, D.K.; Jung, Y.G.; Peterson, I.M.; Lawn, B.R. Cyclic fatigue of intrinsically brittle ceramics in contact with spheres. *Acta Mater.* **1999**, *47*, 4711–4725. [[CrossRef](#)]
22. Sglavo, V.M.; Gadotti, M.; Micheletti, T. Cyclic loading behaviour of soda-lime silicate glass using indentation cracks. *Fatigue Fract. Eng. Mater. Struct.* **1997**, *20*, 1225–1234. [[CrossRef](#)]
23. Morris, D.J.; Cook, R.F. Radial fracture during indentation by acute probes: I, description by an indentation wedging model. *Int. J. Fract.* **2005**, *136*, 237–264. [[CrossRef](#)]
24. Morris, D.J.; Vodnick, A.M.; Cook, R.F. Radial fracture during indentation by acute probes: II, experimental observations of cube-corner and vickers indentation. *Int. J. Fract.* **2005**, *136*, 265–284. [[CrossRef](#)]
25. Wang, W.; Li, Z.; Yao, P.; Li, J.; Chen, F.; Liu, Y. Sink-in/pile-up formation and crack nucleation mechanisms of high purity fused silica and soda-lime silica glass during nanoindentation experiments. *Ceram. Int.* **2020**, *46*, 24698–24709. [[CrossRef](#)]
26. Domnich, V.; Gogotsi, Y.; Dub, S. Effect of phase transformations on the shape of the unloading curve in the nanoindentation of silicon. *Appl. Phys. Lett.* **2000**, *76*, 2214–2216. [[CrossRef](#)]
27. Oliver, D.J.; Bradby, J.E.; Williams, J.S.; Swain, M.V.; Munroe, P. Rate-dependent phase transformations in nanoindented germanium. *J. Appl. Phys.* **2009**, *105*, 126101. [[CrossRef](#)]
28. Rabe, R.; Breguet, J.M.; Schwaller, P.; Staus, S.; Haug, F.J.; Patscheider, J.; Michler, J. Observation of fracture and plastic deformation during indentation and scratching inside the scanning electron microscope. *Thin Solid Film.* **2004**, *469–470*, 206–213. [[CrossRef](#)]
29. Hainsworth, S.V.; McGurk, M.R.; Page, T.F. The effect of coating cracking on the indentation response of thin hard-coated systems. *Surf. Coat. Technol.* **1998**, *102*, 97–107. [[CrossRef](#)]
30. Lawn, B.; Wilshaw, R. Indentation fracture: Principles and applications. *J. Mater. Sci.* **1975**, *10*, 1049–1081. [[CrossRef](#)]
31. Marshall, D.B.; Lawn, B.R.; Evans, A.G. Elastic/Plastic Indentation Damage in Ceramics: The Lateral Crack System. *J. Am. Ceram. Soc.* **1982**, *65*, 561–566. [[CrossRef](#)]
32. Keryvin, V.; Charleux, L.; Hin, R.; Guin, J.P.; Sangleboeuf, J.C. Mechanical behaviour of fully densified silica glass under Vickers indentation. *Acta Mater.* **2017**, *129*, 492–499. [[CrossRef](#)]
33. Ohta, T.; Yan, J.; Kuriyagawa, T.; Kodera, S.; Nakasuji, T. Prediction of subsurface damage depth of ground brittle materials by surface profiling. *Int. J. Mach. Mach. Mater.* **2007**, *2*, 108–124. [[CrossRef](#)]
34. Xiao, H.; Chen, Z.; Wang, H.; Wang, J.; Zhu, N. Effect of grinding parameters on surface roughness and subsurface damage and their evaluation in fused silica. *Opt. Express* **2018**, *26*, 4638–4655. [[CrossRef](#)]
35. Sun, R.; Huang, Y.; Zhang, X.; Zhao, F.; Zhang, Y.; Liu, J.; Hu, J. Study on subsurface damage of fused quartz in grinding stage. In Proceedings of the Eighth Symposium on Novel Photoelectronic Detection Technology and Applications, Kunming, China, 27 March 2022; Proc. SPIE Volume 12169. [[CrossRef](#)]